Journal of Applied Polymer Science

Electrochemical activity of sulfur networks synthesized through RAFT polymerization

C. Almeida,[1] H. Costa,[1] P. Kadhirvel,[1] A. M. Queiroz,[1] R. C. S. Dias,[1] M. R. P. F. N. Costa[2]

[1]LSRE-Instituto Politécnico de Bragança, Department of Chemical and Biological Technology, Quinta de Santa Apolónia, 5300, Bragança, Portugal

[2]LSRE-Faculdade de Engenharia da Universidade do Porto, Department of Chemical Engineering, Rua Roberto Frias s/n, 4200-465, Porto, Portugal

Correspondence to: R. C. S. Dias (E-mail: rdias@ipb.pt)

ABSTRACT: Novel results concerning the inverse vulcanization of sulfur using reversible addition–fragmentation chain transfer (RAFT) polymerization are here reported. It is shown that RAFT polymerization can be used to carry out this crosslinking process, with the additional possibility to extend the reaction time from a few minutes as with classical free radical polymerization (FRP) to several hours. Higher control on viscosity and processability of the synthesized networks, as well as, the implementation of semibatch feed policies during crosslinking are important advantages of the RAFT process here explored comparatively to the FRP inverse vulcanization. Using cyclic voltammetry, it was assessed the electrochemical activity of the synthesized sulfur-rich polymer networks. It is shown that the fundamental electrochemical activity of the elemental sulfur was preserved in the produced materials. Testing of electrochemical cells assembled with lithium in the anode and different sulfur based materials in the cathode, including the synthesized RAFT networks, is also shown. The results here presented highlight the new opportunities introduced by reversible-deactivation radical polymerization mechanisms on the control of the synthesis process and in the design of such advanced materials and show also that many potential derivatizing possibilities can be achieved. © 2016 Wiley Periodicals, Inc. J. Appl. Polym. Sci. **2016**, *133*, 43993.

KEYWORDS: batteries; crosslinking; electrochemistry; fuel cells; inverse-vulcanization; RAFT polymerization

Received 25 January 2016; accepted 29 May 2016
DOI: 10.1002/app.43993

INTRODUCTION

Driven by the high demand in energy storage and conversion, in the last few years, important advances were achieved in the development of batteries. Lithium-ion (Li-ion) systems are in the front edge of these progresses, allowing the production of compact batteries with growing energy densities, important for different kinds of mobile technologies. Nevertheless, applications with very large power intensive needs, such as the electric vehicles, require improved solutions allowing to further increase the energy densities of batteries. However, the cathodes used in Li-ion batteries are often based on ceramic oxides (e.g., cobalt oxide) that restrict additional gains in the energy densities of these devices.[1,2]

Due to particular properties of sulfur (S), namely the relative low atomic weight in comparison with other elements (e.g., cobalt) and the very high specific electron capability that it presents in redox interactions with Li [multielectron transfer reactions are possible for the pair Li/S as generically depicted in eq. (1)], Li–S batteries were explored in the last years aiming at the development of energy storage and conversion systems with improved performance.[3–18] In fact, to the S cathodes is associated a theoretical specific capacity of 1672 mA h g^{-1} and a specific energy of 2600 W h kg^{-1}, which are several times higher than the correspondent to other traditional secondary systems (e.g., 40 W h kg^{-1} for the lead-acid batteries and 150 W h kg^{-1} for Li-ion polymer batteries).[3,4] Moreover, elemental sulfur is nowadays a cheap and available material because it is relatively abundant in nature and appears also as a byproduct of the petroleum refining industry. As consequence, several new technological applications of elemental sulfur are being considered, namely the synthesis of different kinds of advanced materials,[19,20] including improved cathodes for batteries (besides Li–S, Na–S batteries are also being investigated due to the abundance of both latter materials[21])

$$16Li^+ + 16e^- + S_8 \rightleftarrows 8Li_2S \quad (1)$$

In spite of the above mentioned advantages of Li–S batteries, different kinds of issues have a deleterious impact on the performance of such devices. The global electrochemical reaction depicted in eq. (1) involves in fact several complex steps and

intermediate species (e.g., Li_2S_8, Li_2S_4, and Li_2S_2), including the formation of polysulfides (PS) causing the shuttle effect in the electrolyte with concomitant capacity degradation of the battery due to cyclic redox mechanisms involving these PS (see, e.g.,[3,4] and references there in). Moreover, the poor conductivity of S induces a low electrochemical accessibility of the cathodes, and the significant increase of the specific volume in the transition S/Li_2S (0.49–0.60 cm^3 g^{-1}) during the discharge shorten the cycle life of the battery. Additionally, the formation of dendrites is a well-known phenomenon in the Li anodes generating safety problems in batteries. Globally, in consequence of the combination of these effects, Li–S batteries become useless after a few dozen of repeated discharge–charge cycles due to the poor stability of the S cathodes.[3,4]

Different strategies have been considered in the last few years trying to tackle these shortcomings of Li–S electrochemical cells.[3–18] Use of S composite materials[3,4,6,7,9–11,13–18] to improve the conductivity (e.g., including carbon and conductive polymers), change of the electrolyte (e.g., gel electrolytes)[5,6] to minimize the PS shuttle effect or the encapsulation of S considering different architectures (e.g., core–shell and yolk–shell) to increase the stability of the cathodes[3,4,6,8,12,16,17] are examples of research lines that have been explored in this context.

Very recently, a new approach was proposed to increase the stability of the S-based cathodes.[22–26] Through ring-opening polymerization of elemental sulfur (the S_8 ring structure) at high temperature (e.g., 185 °C), in the presence of a crosslinker (e.g., 1,3-diisopropenylbenzene), a sulfur-rich polymer network is formed in a process named inverse vulcanization.[22–26] It was proved that these copolymer networks are electrochemically active and can be used in cathodes of Li–S batteries with enhanced charge capacity and lifetime (1000 mA h g^{-1} and 500 charge–discharge cycles were measured with the produced batteries).[22–26] Moreover, it was showed that these sulfur-rich copolymer networks present interesting properties as high refractive index polymers (HRIP)[22–24,27] with important applications in advanced optoelectronic fabrications (e.g., advanced displays, OLEDs, and antireflective coatings[28–30]). The design of copolymer network composition (through the initial S/crosslinker ratio) is an important issue in order to tailor the properties of the final materials.[24] The front edge of this very recent research line includes also the introduction of new functionalities in the S polymer networks, such as polythiophene segments considering electropolymerization[31] and the direct polymerization of S with poly(3-hexylthiophene-2,5-diyl),[32] the changing of the functionalities of the crosslinker (e.g., using 1,4-diphenylbutadiyene)[33] or the improvement of the processability of the materials through the synthesis of S hyperbranched networks.[34] These researches aimed at the improvement of the performance of cathodes based on S-rich polymer networks, namely by increasing their conductivity and minimizing the PS shuttle effect. The production of sulfur/thiirane copolymers considering reversible addition–fragmentation chain transfer (RAFT) polymerization[35–37] in mild reaction conditions (e.g., temperature range 20–90 °C and in a presence of a solvent), leading to high S content (up to 80%) soluble polymeric materials [e.g., in toluene and tetrahydrofuran (THF)] was also recently reported in literature.[23]

In the research here presented the synthesis of sulfur-rich polymer networks was carried out using the inverse vulcanization process in the presence of a RAFT agent. It is shown that RAFT polymerization can be used to control this crosslinking process, namely concerning the reaction-time evolution and final viscosity of the products. Possibility for the functionalization of S polymer networks with trithiocarbonyl groups is another outcome of the study here reported. Using cyclic voltammetry (CV), it is also shown that the RAFT-synthesized S networks are electrochemically active. Discharge–charge cycling of electrochemical cells assembled with lithium in the anode and different sulfur-based materials in the cathode [elemental sulfur, free radical polymerization (FRP) networks, and RAFT networks] is also reported. Results here presented can be used to design synthesis conditions leading to tailored sulfur-rich polymer networks with applications in cathodes for Li–S batteries, high refractive index materials or heavy metals sorbents.

EXPERIMENTAL

Materials

Elemental sulfur (99.5%; Acros, Geel, Antwerp, Belgium), 1,3-diisopropenylbenzene (DIB, 97%; Sigma-Aldrich, Germany), 2-dodecylthiocarbonothioylthio-2-methylpropionic acid (DDMAT, 98%; Sigma-Aldrich), *S*-(thiobenzoyl)thioglycolic acid (TBTGA, 99%; Sigma-Aldrich), 2,2,6,6-tetramethyl-1-piperidinyloxy (TEMPO, 98% purity; Sigma-Aldrich), conductive carbon (C65; TIMCAL Graphite & Carbon, Brownfieldlaan, Willebroek, Belgium), *N*,*N*-dimethylformamide (DMF, 99.5%; Fisher Scientific, Loughborough, Leicestershire, UK), tetrabutylammonium tetrafluoroborate (TBAB, ≥99% for electrochemical analysis; Fluka Buchs, Switzerland), THF (99.9%; Sigma-Aldrich), chloroform (99%; Sigma-Aldrich), polyethylene (average Mw ~4000 g mol^{-1}; Sigma-Aldrich), perchloric acid (at 70 wt %; Sigma-Aldrich), and DL-dithiothreitol (DTT; ≥99%; Sigma-Aldrich) were used as received. The following materials were used for the assembling of electrochemical cells, aiming at the cycling analysis of batteries incorporating cathodes with the produced S-based networks: split test cells for R&D battery; optional insert size 20 mm of diameter (MTI Corporation, Richmond (CA), USA), Li-ion battery separator film with 25 μm thick trilayer polypropylene–polyethylene–polypropylene membrane (Celgard, Charlotte (NC), USA), conductive carbon coated aluminum foil for battery cathode substrate (MTI Corporation), lithium ribbon, thickness × W 0.38 mm × 23 mm, 99.9% trace metals basis (Sigma-Aldrich), 1,2-dimethoxyethane anhydrous (99.5%; Sigma-Aldrich), 1,3-dioxolane (DIOX) anhydrous (99.8%; Sigma-Aldrich), bis(trifluoromethane)sulfonimide lithium salt (LITFSI, 99.95%; Sigma-Aldrich), and lithium nitrate (Sigma-Aldrich).

Synthesis of Sulfur Polymer Networks

The synthesis of sulfur polymer networks using the classical FRP mechanism was performed using the general method reported in the literature.[22–26] A vial containing the required amount of elemental sulfur and a magnetic stirrer was placed in a thermostatic oil bath stabilized at 185 °C. A yellow liquid was formed in result of sulfur melting (at ~120 °C), and a change to orange color was afterwards observed in result of the S_8 ring opening and radical formation (at ~160 °C). At this point, the

Table I. Initial Compositions Used in the Synthesis of Sulfur Polymer Networks Through FRP and RAFT Polymerization Considering the Inverse-Vulcanization Process with DIB

Material	Weight fraction of S (%) in the S + DIB mixture	Weight fraction of RAFT agent (%) in S + RAFT mixture
S_FRP_1	95	0
S_FRP_2	90	0
S_FRP_3	73	0
S_FRP_4	65	0
S_FRP_5	50	0
S_FRP_6	25	0
S_RAFT_1	90	10.17
S_RAFT_2	90	5.35
S_RAFT_3	90	2.75
S_RAFT_4	90	5.37
S_RAFT_5	90	5.36
S_RAFT_TBTGA	90	3.14
S_NMRP	90	1.18

Final reaction temperature T = 185 °C.

required amount of DIB (a liquid monomer) was added to the melted sulfur and the inverse vulcanization process started. A color change from orange to red indicated the beginning of the crosslinking process that was proceeded under stirring up to the formation of a vitreous material. In Table I are presented the different initial weight fractions of S/DIB considered in these FRP runs (S_FRP_1 to S_FRP_6). A similar procedure was considered in the RAFT crosslinking synthesis, with exception that the required amount of DDMAT (RAFT agent selected) was initially mixed with the elemental sulfur. Weight fractions of reactants used in these RAFT polymerizations are also detailed in Table I (S_RAFT_1 to S_RAFT_5). For comparison purposes, the inverse vulcanization of sulfur was also performed in the presence of the dithiobenzoate RAFT agent TBTGA (run S_RAFT_TBTGA) and considering nitroxide-mediated radical polymerization (NMRP) in the presence of the stable radical TEMPO (run S_NMRP).

Cleavage of the Sulfur Networks Using DTT

The effective formation of sulfur-sulfur bonds was confirmed by reductive cleavage of the produced S/DIB copolymers using DTT. These reductive cleavage reactions were performed by adding about 200 mg of DTT to 100 mg of sulfur polymer network in an Erlenmeyer flask under argon atmosphere. Later, 10 mL of deoxygenated THF were added, and the resulting solution was stirred at room temperature and sampled along the reaction time (up to 210 min final time). Samples withdrawn were diluted in THF for analysis by size exclusion chromatography (SEC/RI/MALLS) in order to monitor the cleavage process.

Product Analysis by SEC/RI/MALLS

Reaction samples were diluted in THF, and after a period of least 24 h, the soluble material was filtered to be injected in the SEC/RI/MALLS system. The used SEC/RI/MALLS apparatus is composed of a Polymer Laboratories PL-GPC-50 integrated SEC system with differential refractometer working at 950 ± 30 nm, attached to a Wyatt Technology DAWN8$^+$ HELEOS 658 nm MALLS detector. A train of three GPC columns PL gel (300 mm × 7.5 mm) with nominal particle size 10 μm and pore type MIXEDB-LS was used. Analyses were performed at 30 °C with THF as the eluent at a flow rate of 1 mL min^{-1}.

FTIR Analysis

FTIR analyses of selected products were performed after drying of the samples. The powdered materials were then mixed with KBr and pressed into pellets in order to collect the corresponding IR spectra.

CV Measurements

CV measurements were performed using a Zahner Xpot potentiostat with a potential range of ±10 V (potential accuracy = ±1 mV) and current range from ±10 nA to ±500 mA (current accuracy = ±100 pA). Voltammograms were collected using the software package Power-Potentiostats Inspector V 8.1. Different electrode combinations were used in the CV measurements including the Ag/AgCl reference electrode (SE 11 NSK-7; Sensortechnik Meinsberg GmbH, Meinsberg, Waldheim, Germany), platinum counter electrode (surface area = 4 cm^2, Ref. SE 11 NSK-7; Sensortechnick Meinsberger), platinum working electrode (2 mm diameter, Ref. 6.1204. 120; Metrohm AG, Ionenstrasse, Herisau, Switzerland), glassy carbon working electrodes (2 mm diameter, Ref. 6.1204. 600; Metrohm). Homemade graphite and steel electrodes (4 mm diameter) were also used in CV experiments. The optimized conditions for these CV electrochemical analyses were observed using an organic solution of 0.1*M* TBAB in DMF as electrolyte. Other possibilities were tested, including a 0.1*M* perchloric acid aqueous solution.

The characterization of the electrochemical activity of the sulfur polymer networks was performed by casting a paste containing the selected material on the surface of the working electrode. With this purpose, the sulfur-based material was combined with conductive carbon and polyethylene (working as a binder) in the mass ratios 75/20/5, respectively. These components were milled in the presence of chloroform in order to obtain a slurry. The active end of the electrode was dip into the slurry, and after drying, a surface coated with the mixture containing the sulfur polymer network was ready to be used in the CV measurements.

Assembling of Electrochemical Cells and Cycling Battery Analysis

The electrochemical studies were performed in Split Test Cell type devices with an optional insert size of 20 mm diameter (MTI Corporation). The assembly of electrochemical cells has been carried out in a glove box filled with dry argon. The positive electrodes were fabricated by mixing the active materials (sulfur polymer networks or elemental sulfur) with conductive carbon and polyethylene as a binder in a mass ratio of, respectively, 75/20/5 and milled into slurry as described above in the CV testing. The slurry was then blade cast onto conductive carbon-coated aluminum foil, dried in air, and finally cut in round discs of 13 mm diameter. The sulfur load obtained was typically in the range 1–2 mg cm^{-2}. Negative electrodes have been made from lithium metal, cut in 16 mm diameter round

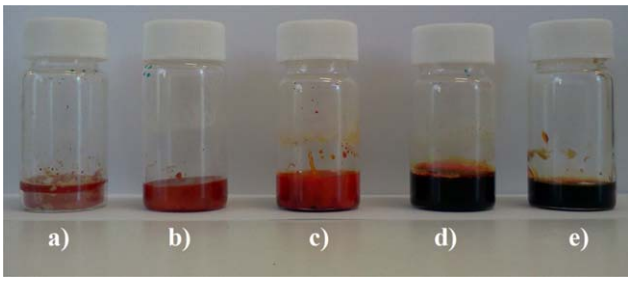

Figure 1. Photographs of the final products obtained in different FRP runs concerning the inverse vulcanization of S/DIB: (a) 95%, (b) 90%, (c) 65%, (d) 50%, and (e) 25% S. [Color figure can be viewed in the online issue, which is available at wileyonlinelibrary.com.]

discs 0.38 mm thick. A solution containing 0.38*M* LITFSI + 0.31*M* lithium nitrate in a (1:1, v/v) mixture of DIOX and 1,2-dimethoxyethane was used as electrolyte in the electrochemical cells.[22] Freshly prepared and purged (for oxygen removing) electrolytes were used with the different assembled electrochemical cells. A 20-mm diameter and 25-μm thick trilayered polypropylene–polyethylene–polypropylene film was used to separate anode and cathode. The separator was soaked in 75 μL electrolyte solution for 3 h before cell assembling. After assembly of the electrochemical cell, the open-circuit voltage (V_{OC}) was measured to ensure a potential between 2.3 and 2.5 V before the galvanostatic charge–discharge measurements. Battery cycling (galvanostatic charge–discharge analysis) was performed using the aforementioned Zahner Xpot potentiostat working from 1.7 to 2.6 V.

RESULTS AND DISCUSSION

Polymerization runs as described in Table I were planned in order to assess the effect of the initial composition and of the use of reversible-deactivation radical polymerization (RDRP) techniques on the control of the crosslinking process and on the properties of the final sulfur networks. In conventional FRP synthesis, the initial weight fraction of sulfur was lowered from 95% to 25%. Fast reactions are observed with high initial sulfur content, and a vitreous material is formed within a few minutes, blocking the mixture stirring. Sluggish changes in the viscosity of the reaction medium are observed at lower sulfur content reaction systems. Blocking of the stirring magnetic bar was observed after 3.7, 4.0, 6.0, and 7.3 min with 95%, 90%, 73%, and 65% S content, respectively. Stirring up to at least 25 min was possible with the 50% and 25% S products; the polymerizations were stopped at this reaction time. After cooling, final materials are opaque in the composition range 65%–95% S and look translucent between 50% and 25% S. These latter two materials present viscoelasticity even after cooling to room temperature. Photographs of the final products obtained in different FRP runs concerning the inverse vulcanization of S/DIB are presented in Figure 1. Note that compositions usually considered in the production of sulfur-based HRIP are in the range 50%–80% S,[27] whereas the best weight fraction of sulfur for S cathode materials was found to be around 90% S.[25]

Thus, considering that this research is also focused on the electrochemical activity of sulfur-rich networks, studies on the

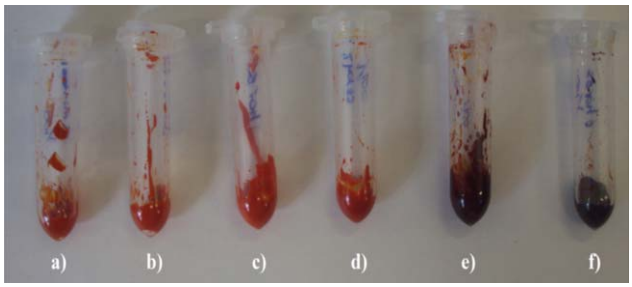

Figure 2. Photographs of the products correspondent to the sampling of the reaction mixture in a RAFT run concerning the inverse vulcanization of S/DIB (run S_RAFT_3 with 2.75% DDMAT, as described in Table I). Sampling times: (a) 15 min, (b) 30 min, (c) 1 h, (d) 2 h, (e) 4 h, and (f) 6 h. [Color figure can be viewed in the online issue, which is available at wileyonlinelibrary.com.]

inverse vulcanization of sulfur considering RDRP mechanisms were performed using the 90% S as reference. Using DDMAT as the RAFT agent and choosing the initial weight fraction in the range 2.75%–10.17% (see Table I), it was always possible to extend the crosslinking process up to at least 6 h while keeping good stirring conditions of the reaction mixture. A clear contrast between the FRP and RAFT inverse vulcanization of sulfur is therefore observed in these conditions and an easy control of the process is possible with the latter polymerization technique. Sampling of the viscous mixture was also possible along the reaction time when using RAFT with DDMAT, as depicted in Figure 2 where the photographs of products correspondent to 15 min, 30 min, 1 h, 2 h, 4 h, and 6 h of polymerization are showed.

Opaque products were obtained with the three RAFT compositions tested in all sampling times. This should be the consequence of the 90% S weight fraction in the S + DIB mixture, similarly to the FRP experiments above described. Only with about S <50% S translucent materials are formed. Note that besides the improved control of the crosslinking process, the inclusion of the RAFT agent can be used to synthesize functionalized sulfur networks. The design of the degree of functionalization can be achieved by changing the initial weight fraction of RAFT agent in the starting mixture, as reported in Table I. In the present work, the eventual impact of the RAFT content in the electrochemical properties of the obtained materials will be assessed below.

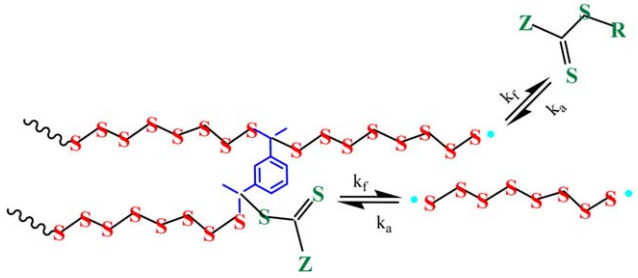

Figure 3. Depiction of the inverse vulcanization of sulfur using RAFT polymerization. Control of the crosslinking process is possible in the presence of a suitable RAFT agent. Functionalization of the networks through the RAFT groups is another outcome that can be further explored in new synthesis paths. [Color figure can be viewed in the online issue, which is available at wileyonlinelibrary.com.]

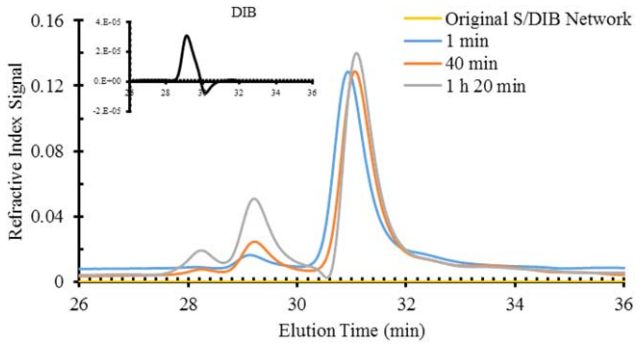

Figure 4. SEC traces correspondent to the soluble material of a FRP synthesized S/DIB network (90% S) and the products resulting from its reductive cleavage with DTT. Analysis of samples correspondent to different reductive cleavage times (1 min, 40 min, and 1 h and 20 min) are presented. For comparative purposes, the SEC analysis of DIB is also included. [Color figure can be viewed in the online issue, which is available at wileyonlinelibrary.com.]

Figure 3 depicts the inverse vulcanization of sulfur using RAFT polymerization. The control of the crosslinking process arises from the reversible radical activation and fragmentation mechanisms that become effective when a suitable RAFT agent is selected (specific effect of the Z and R chemical groups).[35–37] Many dormant polymer chain ends are formed when the RAFT polymerization is efficient. These reactive terminal groups (stopping and restarting the polymerization) can be purposely used to promote further polymerization steps and to functionalize the produced materials. The new reaction paths provided with RAFT polymerization can be exploited to include in the networks other moieties improving the performance of S-based cathodes, as considered in refs. 31 and 32 using different approaches. Moreover, other applications of S networks are currently being reported in the scientific community, namely the synthesis of high refractive index materials[38] or heavy metals sorbents.[39,40] Within these latter classes of materials, increasing of the processability and/or functionalization to improve the sorption capability are achievements that can be further explored with RAFT polymerization.

The control of the inverse vulcanization of sulfur was also tried using TBTGA as RAFT agent (a cheaper chemical in comparison with DDMAT), as described in Table I. However, a poor control of the process was observed in the reported conditions and a fast reaction comparable to the FRP process resulted. Note that TBTGA and RAFT agents present very different Z and R substitutes (see Figure 3), with DDMAT belonging to the class of trithiocarbonates and TBTGA to the dithiobenzoates. The values of the transfer constants between polymer radicals (here S or DIB derived) and the dormant species, which are affected by the chemical groups Z and R, should preclude the effective control of the vulcanization process using TBTGA. Indeed, poor control of network formation in the presence of TBTGA, considering other chemical systems, has been recently reported in the literature.[36] For comparison purposes, the control of this crosslinking system was also studied considering a NMRP in the presence of TEMPO (see Table I). Once again, a poor control of the process was achieved likely due to the ineffective reversible end-capping of S radicals by TEMPO (it is known that NMRP is more effective with styrene monomers). Note that failure of TEMPO to perform the reversible deactivation of the sulfur-centered radicals here reported is also often observed with monomers, such as acrylates and methacrylates.[37] The control of the formation process of S networks and their functionalization is possible using RAFT with DDMAT, as described above, but there is an important room for improvement in this domain.[23]

The effective formation of sulfur–sulfur bonds in the different kinds of networks synthesized in this work was investigated considering the reductive cleavage of the produced S/DIB copolymers using DTT.[22] The soluble part (in THF) of the synthesized networks and products resulting from the reductive cleavage of these materials were analyzed using SEC. Comparison of the different SEC traces observed highlights the presence of S—S bonds in the networks, as shown in Figure 4 for a FRP synthesized S/DIB network (90% S). Indeed, the presence of THF soluble materials is practically undetectable in the original network. However, the appearance of soluble species in the chromatograms of samples correspondent to increasing reductive cleavage times shows that there is a breaking process of the S—S bonds in the network. A similar analysis is shown in Figure 5 where the chromatographic trace in THF of the original RAFT synthesized S/DIB network is compared with the SEC traces correspondent to samples submitted to increasing reductive cleavage times. Note the very high RI signal correspondent to the 3 h 30 min sampling time pointing to a very high concentration of soluble species arising from the breakage of the S—S bonds.

Taking advantage from the easy sampling of the reaction mixture along the inverse vulcanization process when using RAFT, the evolution of network formation along the reaction time and temperature was also investigated using the SEC analysis of the soluble material in THF, as depicted in Figure 6. In spite of the low intensity of observed RI signal (low content of soluble material), the time/temperature evolution of low and high size species intervenient in the crosslinking process can be followed. Note that in the final product (6 h reaction time) the weight

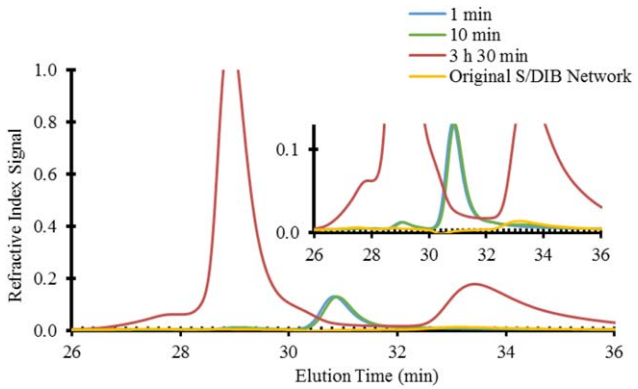

Figure 5. SEC traces correspondent to the soluble material of a RAFT synthesized S/DIB network (90% S and 5.35% DDMAT) and the products resulting from its reductive cleavage with DTT. Analysis of samples correspondent to different reductive cleavage times (1 min, 10 min, and 3 h and 30 min) are presented. [Color figure can be viewed in the online issue, which is available at wileyonlinelibrary.com.]

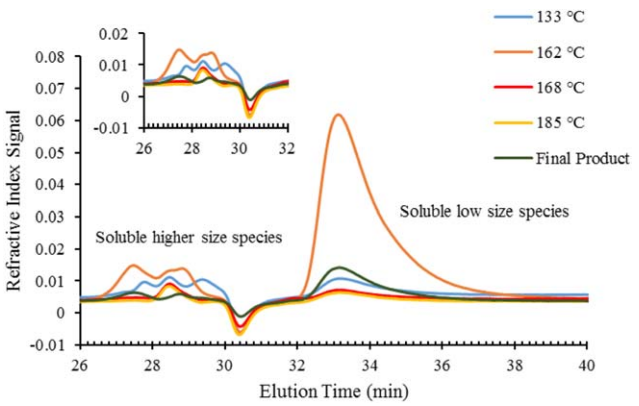

Figure 6. SEC traces correspondent to the soluble material of samples withdrawn at different temperatures during RAFT synthesis of an S/DIB network (90% S and 5.35% DDMAT). Results correspondent to the sampling at 133 °C, 162 °C, 168 °C, and 185 °C and the final product after 6 h reaction time (also at 185 °C) are presented. [Color figure can be viewed in the online issue, which is available at wileyonlinelibrary.com.]

fraction of soluble material is very low. Results presented in Figures 4–6 are an indirect evidence for the formation of sulfur networks both using FRP and RAFT polymerization. However, additional kinetic studies are needed in order to have a clear picture on the reaction mechanisms involved in the inverse vulcanization process using RAFT polymerization. Selection of different kinds of RAFT agents allowing the control of the process and change of the initial proportions between sulfur/crosslinker/RAFT agent are some important parameters to be considered in these studies. Final applications of the S networks (e.g., electrochemical, high refractive index materials, and heavy metals sorbents, as discussed above) should also guide such studies.

With high sulfur content networks (e.g., S >80%) only limited information can be obtained using FTIR analysis, as shown in Figure 7. Comparing the FTIR spectrum of the DIB crosslinker with those correspondent to S networks with different sulfur content, it is shown that some characteristic responses of the organic monomer can be clearly observed in the 73% S networks (e.g., 718 and 800 cm^{-1} peaks correspondent to DIB ring

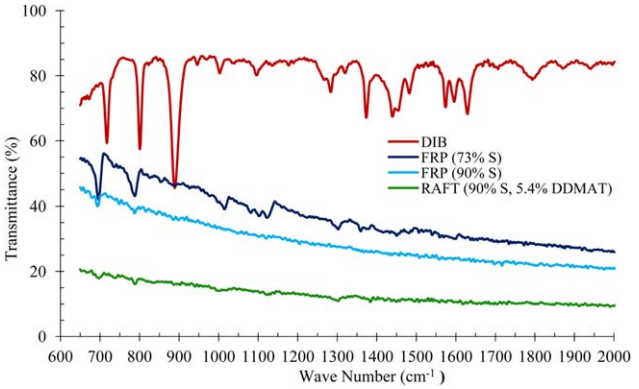

Figure 7. FTIR analyses of the DIB monomer and sulfur-rich polymer networks synthesized considering different S/DIB compositions and also different polymerization mechanisms (FRP and RAFT). [Color figure can be viewed in the online issue, which is available at wileyonlinelibrary.com.]

vibrational assignments), but a tiny response is observed for the 90% S networks in these regions. However, the peak in the crosslinker spectrum at 900 cm^{-1}, including the $=CH_2$ wag vibrational assignment, cannot be identified in the networks; this is consistent with a high consumption of the double bonds during the crosslinking process. Thus, the formation of S-networks both for FRP and RAFT polymerization seems also to be indicated from the FTIR analysis of analogue products. Moreover, the thermal gravimetric analysis (TGA) of elemental sulfur and different polymerization products presented in Figure 8 also supports this assumption. Indeed, an important effect of the crosslinker content in TGA profiles is observed, as previously reported in the literature for FRP networks,[22,33] whereas a similar thermal degradation was observed in our research for FRP and RAFT products with equivalent DIB content.

The assessment of the electrochemical activity of the prepared S/DIB networks was performed using the CV technique. Note that the electrochemical activity of S/DIB copolymers is a central issue in the context of the usage of these materials in cathodes for Li–S batteries. The proposed mechanism supporting the electrochemistry of the S/DIB networks in Li–S batteries involves high and low voltages plateaus and different kinds of lower order sulfide products, such as Li_2S_8, Li_2S_4, Li_2S_3, and Li_2S_2.[25] High-order organosulfur networks (number of S atoms in the network branches $x \sim 8$) and Li_2S_8 are postulated to be formed at the high-voltage plateau. In an intermediate discharge plateau, these species are transformed in $x \sim 3$ networks and Li_2S_4, which becomes later fully discharged ($x \sim 1$ networks + Li_2S_3 + Li_2S_2) in the low-voltage plateau.[25]

In the present work, the comparison of the electrochemical activity of the elemental sulfur and of the S/DIB networks, both measured by the CV technique, was considered in order to show that the synthesized materials preserve the fundamental features allowing their incorporation in cathodes for Li–S batteries. In Figure 9

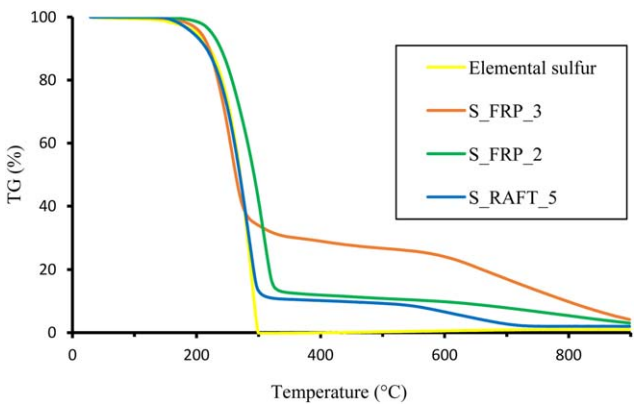

Figure 8. TGA of elemental sulfur and different S-DIB networks synthesized through FRP and RAFT polymerization. The comparison between the thermal degradation of elemental sulfur and the different polymer products highlight the effect of the crosslinking. The amount of DIB has an important impact on the thermal degradation of the networks (comparison S_FRP_3/S_FRP_2) but similar profiles are observed for FRP and RAFT synthesized products with the same amount of DIB (comparison S_FRP_2/S_RAFT_5). [Color figure can be viewed in the online issue, which is available at wileyonlinelibrary.com.]

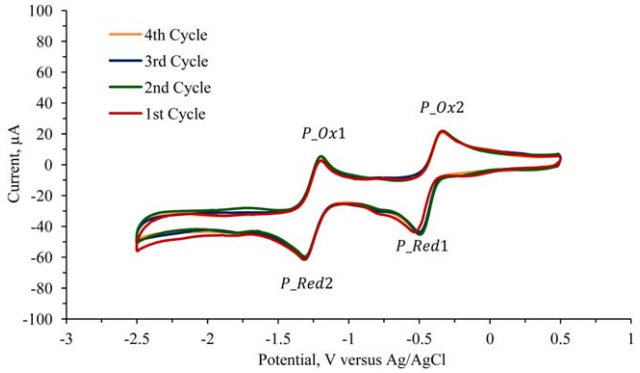

Figure 9. Cyclic voltammograms of elemental sulfur in a DMF solution containing 0.1*M* TBAB and 2 m*M* S_8. Four cycles are showed. Analysis conditions: scan rate = 50 mV s^{-1}, reference electrode = Ag/AgCl, and working and counter electrodes = glassy carbon. [Color figure can be viewed in the online issue, which is available at wileyonlinelibrary.com.]

are presented the cyclic voltammograms of elemental sulfur in a DMF solution containing 0.1*M* TBAB and 2 m*M* S_8. Note that the selection of the proper experimental conditions (e.g., the electrolyte and used electrodes) is a key factor in order to achieve good description of the electrochemical activity of this system, as reported in fundamental researches is this area.[41,42] In the CV analysis presented in Figure 9 are clearly identified the fundamental redox processes involving elemental sulfur,[41,42] namely

$$\text{Peak } P_{red1}\text{: } S_8 + 2e^- \rightarrow S_8^{2-} \quad (2)$$

$$S_8^{2-} \rightarrow 2S_4^-$$

$$\text{Peaks } P_{red2}/P_{ox1}\text{: } 2S_4^- + 2e^- \rightleftarrows 2S_4^{2-} \quad (3)$$

$$\text{Peak } P_{ox2}\text{: } 2S_4^- \rightarrow 2S_4 + 2e^- \quad (4)$$

$$2S_4 \rightarrow S_8$$

In Figure 10 are presented the cyclic voltammograms for pastes containing an S/DIB polymer network synthesized by RAFT

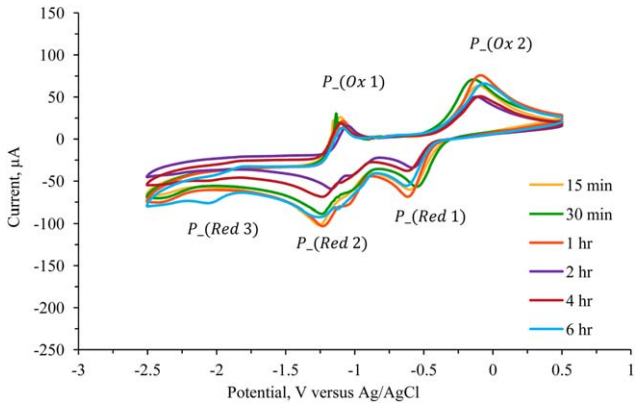

Figure 10. Cyclic voltammograms for pastes containing an S/DIB polymer network synthesized by RAFT (90% S and 10.17% DDMAT). The CV of pastes correspondent to different sampling times during the inverse vulcanization process are showed (15 min to 6 h). Analysis conditions: electrolyte: DMF solution containing 0.1*M* TBAB, scan rate = 50 mV s^{-1}, reference electrode = Ag/AgCl, and working and counter electrodes = glassy carbon. [Color figure can be viewed in the online issue, which is available at wileyonlinelibrary.com.]

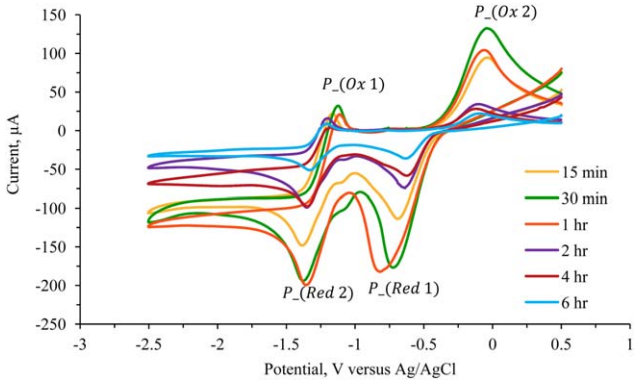

Figure 11. Cyclic voltammograms for pastes containing an S/DIB polymer network synthesized by RAFT (90% S and 5.35% DDMAT). The CV of pastes correspondent to different sampling times during the inverse vulcanization process are showed (15 min to 6 h). Analysis conditions: electrolyte: DMF solution containing 0.1*M* TBAB, scan rate = 50 mV s^{-1}, reference electrode = Ag/AgCl, and working and counter electrodes = glassy carbon. [Color figure can be viewed in the online issue, which is available at wileyonlinelibrary.com.]

polymerization (90% S and 10.17% DDMAT). The CV of pastes formed with sulfur polymeric materials corresponding to different sampling times during the RAFT inverse vulcanization process are shown (15 min to 6 h). Comparison of these CV analyses with those presented in Figure 9 allows to conclude that the fundamental electrochemical properties of the elemental sulfur were preserved after the network formation through the RAFT inverse vulcanization process. These fundamental electrochemical mechanisms [described by eqs. (2–4)] are observable in all the sulfur polymeric materials, regardless of the reaction time. These conclusions are also confirmed through the results presented in Figures 11–13 where the CV of pastes containing sulfur networks synthetized with 5.35% DDMAT, 2.75% DDMAT, and using FRP, respectively, is presented. Note that the shape of the cyclic voltammograms observed (e.g., peaks

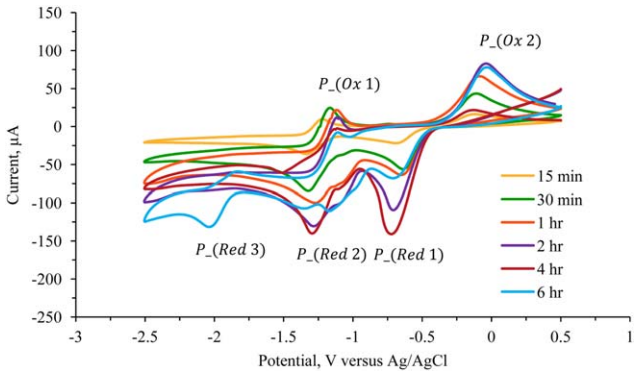

Figure 12. Cyclic voltammograms for pastes containing an S/DIB polymer network synthesized by RAFT (90% S and 2.75% DDMAT). The CV of pastes correspondent to different sampling times during the inverse vulcanization process are showed (15 min to 6 h). Analysis conditions: electrolyte: DMF solution containing 0.1*M* TBAB, scan rate = 50 mV s^{-1}, reference electrode = Ag/AgCl, and working and counter electrodes = glassy carbon. [Color figure can be viewed in the online issue, which is available at wileyonlinelibrary.com.]

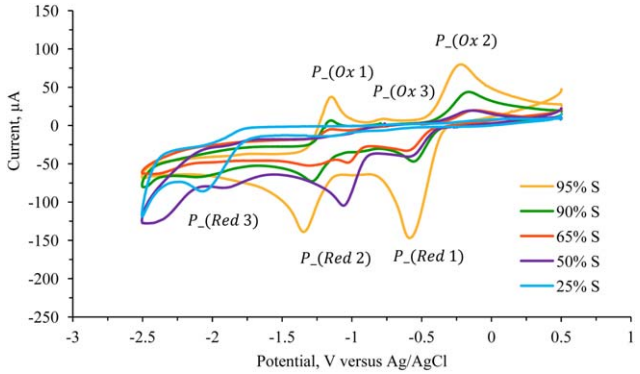

Figure 13. Cyclic voltammograms for pastes containing an S/DIB polymer network synthesized by FRP. The CV of pastes correspondent to different S/DIB initial compositions are showed (95–25% S). Analysis conditions: electrolyte: DMF solution containing 0.1*M* TBAB, scan rate = 50 mV s^{-1}, reference electrode = Ag/AgCl, and working and counter electrodes = glassy carbon. [Color figure can be viewed in the online issue, which is available at wileyonlinelibrary.com.]

position, width, and height) is affected by several conditions of the CV analysis, including reversible diffusion phenomena of species in the electrolyte towards the working electrode. Homogeneity of the produced pastes including the sulfur-rich networks and thickness of layer applied in the working electrode can also affect the observed cyclic voltammograms with the different materials. In spite of these differences in the shape of the observed cyclic voltammograms, the fundamental electrochemical mechanisms of elemental sulfur described by eqs. (2–4) are clearly identified with all the polymer networks tested.

Additional features of the electrochemical activity of elemental sulfur are also observed in some CV of S networks tested, namely the reduction peak P_{red3} (see Figures 10, 12 and 13) and the oxidation peak P_{ox3} (see Figure 13). It is reported in the literature[41,42] that the P_{red3} peak correspond to the following mechanism:

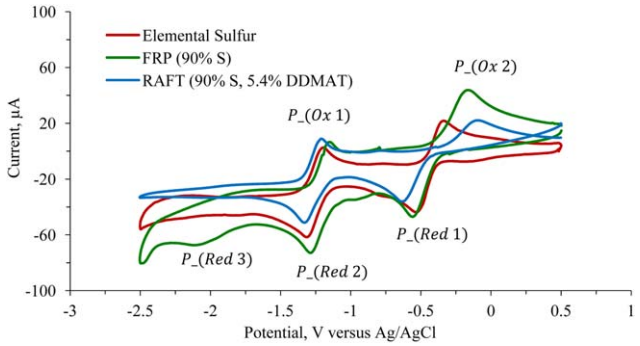

Figure 14. Comparison of the cyclic voltammograms of the elemental sulfur and pastes containing an S/DIB polymer networks synthesized by FRP and RAFT. Analysis conditions: electrolyte: DMF solution containing 0.1*M* TBAB, scan rate = 50 mV s^{-1}, reference electrode = Ag/AgCl, and working and counter electrodes = glassy carbon. The electrolyte solution includes 2 m*M* S_8 in the analysis of the electrochemical activity of elemental sulfur. [Color figure can be viewed in the online issue, which is available at wileyonlinelibrary.com.]

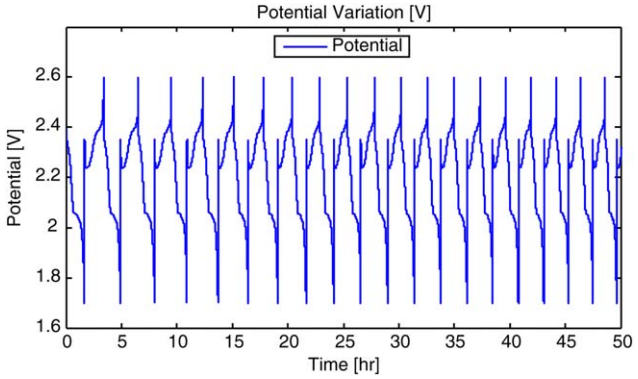

Figure 15. Observed discharge-charge cycling for an electrochemical cell assembled with lithium in the anode and a FRP synthesized sulfur network in the cathode (S_FRP_2). Measurements were performed between the potential values of 1.7 and 2.6 V and at the rate of C/4. [Color figure can be viewed in the online issue, which is available at wileyonlinelibrary.com.]

$$\text{Peak } P_{red3}: \quad S_8^{2-} + 2e^- \rightarrow S_8^{4-} \qquad (5)$$
$$S_8^{4-} \rightarrow \text{products}$$

The electrochemical mechanism originating the peak P_{ox3} in elemental sulfur is not consensual in the scientific community, and it is reported that it can be only observed in specific CV analysis conditions.[41]

In Figure 14 are compared the cyclic voltammograms observed with the elemental sulfur and pastes containing an S/DIB polymer networks synthesized through FRP and RAFT polymerization, both with 90% S. The conservation of the electrochemical activity of elemental sulfur in the networks synthesized in the assigned conditions becomes again clear with this comparison. Notice that, as expected, for a too low sulfur content of the polymer networks, the electrochemical activity of the materials decreases, as can be observed with the results presented in Figure 13.

In Figures 15–19 are presented the results obtained with the testing of electrochemical cells assembled with lithium in the anode and different sulfur-based materials in the cathode (elemental sulfur, FRP networks, and RAFT networks). In Figures

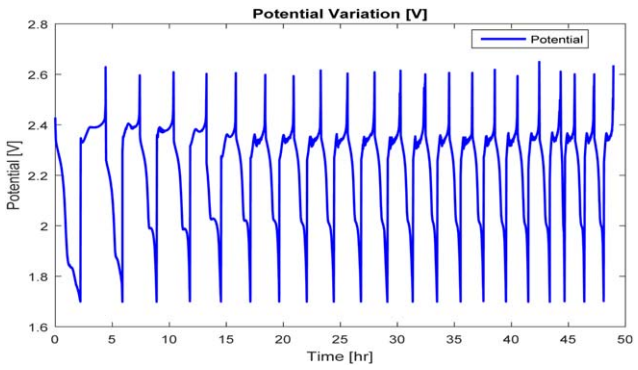

Figure 16. Observed discharge-charge cycling for an electrochemical cell assembled with lithium in the anode and a RAFT synthesized sulfur network in the cathode (S_RAFT_5). Measurements were performed between the potential values of 1.7 and 2.6 V and at the rate of C/4. [Color figure can be viewed in the online issue, which is available at wileyonlinelibrary.com.]

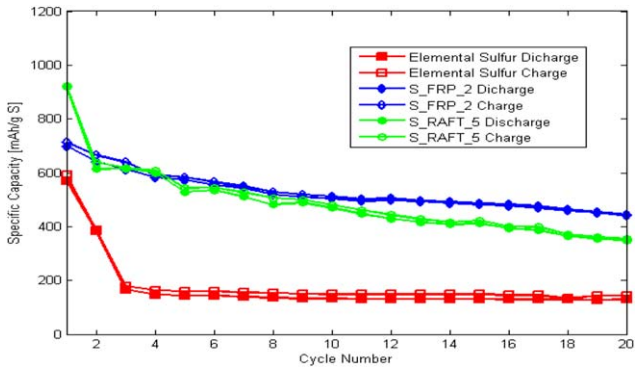

Figure 17. Cycling performance of electrochemical cells assembled with lithium in the anode and different sulfur based materials in the cathode (elemental sulfur, FRP synthesized networks and RAFT synthesized networks are compared). Measurements were performed between the potential values of 1.7 and 2.6 V and at the rate of C/4. [Color figure can be viewed in the online issue, which is available at wileyonlinelibrary.com.]

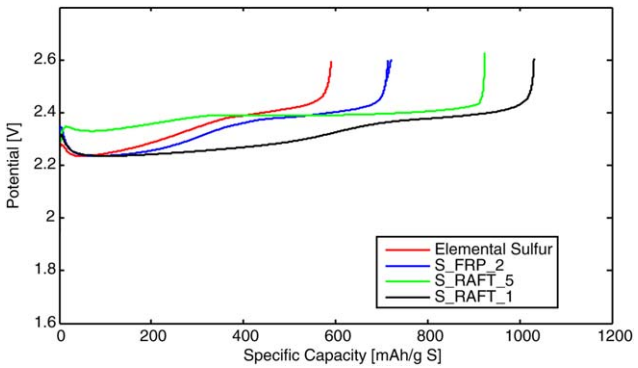

Figure 19. Charge profiles observed in the first cycle for electrochemical cells assembled with lithium in the anode and elemental sulfur, FRP synthesized sulfur network (S_FRP_2) and different RAFT synthetized sulfur networks (S_RAFT_1 and S_RAFT_5) in the cathode. Measurements were performed between the potential values of 1.7 and 2.6 V and at the rate of C/4. [Color figure can be viewed in the online issue, which is available at wileyonlinelibrary.com.]

15 and 16 is shown that batteries incorporating FRP and RAFT synthesized S networks in the cathode exhibit similar ability to be submitted to discharge–charge cycling.

Figure 17 compares the cycling performance of electrochemical cells assembled with elemental sulfur, FRP, and RAFT-synthesized networks, highlighting the improved performance that is observed both with FRP and RAFT products comparatively to the elemental sulfur. These results are consistent with the enhancement of cycling stability reported with FRP polymers[22–26] and also show similar accomplishments for RAFT products. In Figure 18 are compared the discharge and charge profiles observed in the 1st and 20th discharge–charge cycles for electrochemical cells assembled with FRP or RAFT synthetized sulfur networks in the cathode. In Figure 19 are compared the charge profiles observed in the 1st cycle for electrochemical cells assembled with different materials, including RAFT networks obtained with unequal DDMAT

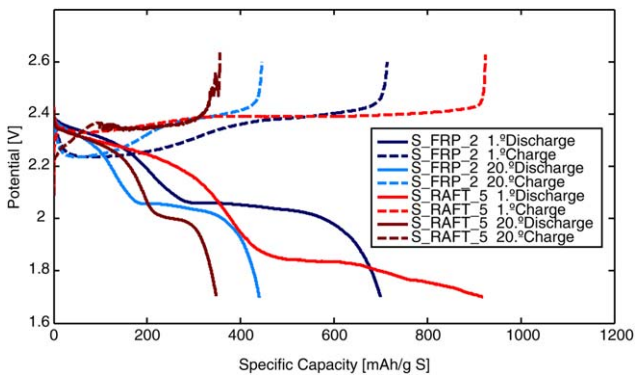

Figure 18. Discharge and charge profiles observed in the 1st and 20th discharge-charge cycles for electrochemical cells assembled with lithium in the anode and FRP or RAFT synthetized sulfur networks in the cathode (S_FRP_2 or S_RAFT_5). Measurements were performed between the potential values of 1.7 and 2.6 V and at the rate of C/4. [Color figure can be viewed in the online issue, which is available at wileyonlinelibrary.com.]

amount. Note that specific capacity values up to 1000 mA h g^{-1} S were measured in the first cycle with some assembled cells (see Figure 19), which is a good result in the framework of other related researches.[4,22–26]

Initial specific capacity of the cells seems to be improved when sulfur networks synthesized with higher amounts of DDMAT are used (see Figure 19). These results should be the consequence of the higher solubility in the electrolyte of the PS formed through RAFT polymerization when the amount of RAFT agent is increased. Note that the primary chain length is shorter with RAFT polymerization than with FRP and is further shortened when increasing the amount of RAFT agent. It is reported that high PS solubility favors the cell reaction but imposes a negative impact on coulombic efficiency and capacity retention.[4] Indeed, decreasing of specific capacity with cycling was always observed (see Figure 18), showing the need for further improvements in the electrochemical cells and cathode materials. The performance of these cells is affected by many other factors, such as the carbon/sulfur ratio, sulfur loading, kind and amount of electrolyte, and cycling rate. Hence, further studies changing the cell conditions, namely using a lower charge/discharge rate (e.g., C/10) and considering other architectures (e.g., coin cells), should be performed in order to achieve final conclusions concerning the impact of RAFT networks on the electrochemical performance of such devices.

CONCLUSIONS

It was shown that the inverse vulcanization of sulfur can be controlled using RAFT polymerization in the presence of DDMAT. The crosslinking process for the production of networks with high sulfur content (e.g., 90%) was extended from a few minutes with classical FRP to up to 6 h with RAFT in the presence of DDMAT. Formation of sulfur networks, both with FRP and RAFT polymerization, was put into evidence through reductive cleavage, FTIR, and TGA of the products. Improved regulation of the viscosity and processability of the materials,

implementation of semibatch feed policies during the inverse vulcanization process, and functionalization of the sulfur networks are some opportunities introduced with RAFT polymerization. These new reaction pathways can be explored to tailor products with applications in electrochemistry, as high refractive index materials or heavy metals adsorbents.

Using CV, it was shown that the fundamental electrochemical activity of the elemental sulfur was preserved in the produced S networks, considering FRP or RAFT polymerization. Electrochemical cells with lithium in the anode and different sulfur-based materials in the cathode (elemental sulfur, FRP networks, and RAFT networks) were assembled and tested with discharge–charge cycling. Enhancement of cycling stability comparatively to elemental sulfur was observed both with FRP and RAFT networks. Improved initial specific capacity was also observed when using sulfur networks synthesized with higher amounts of DDMAT. Higher solubility in the electrolyte of the PS formed through RAFT polymerization should be at the source of this initial improvement but decreasing of specific capacity with cycling was always observed. Further studies changing the cell conditions, namely the used discharge/charge rate, electrolyte, and device architecture should be performed in order to achieve final conclusions concerning the impact of RAFT networks on the electrochemical performance of the batteries.

ACKNOWLEDGMENTS

The authors thank FCT and FEDER under Programme COMPETE (Project PEst-C/EQB/LA0020/2013), QREN, ON2, and FEDER (Project NORTE-07-0162-FEDER-000050), and QREN, ON2, and FEDER (Project NORTE-07-0124-FEDER-0000014—Polymer Reaction Engineering). We acknowledge TIMCAL Graphite & Carbon for supplying the conductive carbon C65. This work was also financially supported by Project POCI-01-0145-FEDER-006984 – Associate Laboratory LSRE/LCM funded by FEDER funds through COMPETE2020 – Programa Operacional Competitividade e Internacionalização (POCI) – and by national funds through FCT – Fundação para a Ciência e a Tecnologia.

REFERENCES

1. Xu, G.; Ding, B.; Pan, J.; Nie, P.; Shen, L.; Zhang, X. *J. Mater. Chem. A* **2014**, *2*, 12662.
2. Ellis, B. L.; Lee, K. T.; Nazar, L. F. *Chem. Mater.* **2010**, *22*, 691.
3. Chen, R.; Zhao, T.; Feng, W. *Chem. Commun.* **2015**, *51*, 18.
4. Ding, N.; Chien, S. W.; Hor, T. S. A.; Liu, Z.; Zong, Y. *J. Power Sources* **2014**, *269*, 111.
5. Scheers, J.; Fantini, S.; Johansson, P. *J. Power Sources* **2014**, *255*, 204.
6. Xu, G. L.; Wang, Q.; Fang, J. C.; Xu, Y. F.; Li, J. T.; Huang, L.; Sun, S. G. *J. Mater. Chem. A* **2014**, *2*, 19941.
7. Wang, J.; He, Y. S.; Yang, J. *Adv. Mater.* **2015**, *27*, 569.
8. Wu, F.; Chen, J.; Chen, R.; Wu, S.; Li, L.; Chen, S.; Zhao, T. *J. Phys. Chem. C* **2011**, *115*, 6057.
9. Wu, F.; Wu, S.; Chen, R.; Chen, J.; Chen, S. *Electrochem. Solid State Lett. A* **2010**, *13*, 29.
10. Choi, Y. J.; Chung, Y. D.; Baek, C. Y.; Kim, K. W.; Ahn, H. J.; Ahn, J. H. *J. Power Sources* **2008**, *184*, 54.
11. Wang, J.; Yang, J.; Wan, C.; Du, K.; Xie, J.; Xu, N. *Adv. Funct. Mater.* **2003**, *13*, 487.
12. Seh, Z. W.; Li, W.; Cha, J. J.; Zheng, G.; Yang, Y.; McDowell, M. T.; Hsu, P. C.; Cui, Y. *Nat. Commun.* **2013**, *4*, 1.
13. Ji, X.; Lee, K. T.; Nazar, L. F. *Nat. Mater.* **2009**, *8*, 500.
14. Han, S. C.; Song, M. S.; Lee, H.; Kim, H. S.; Ahn, H. J.; Lee, J. Y. *J. Electrochem. Soc. A* **2003**, *150*, 889.
15. Zheng, S.; Wen, Y.; Zhu, Y.; Han, Z.; Wang, J.; Yang, J.; Wang, C. *Adv. Energy Mater.* **2014**, *4*, 1400482.
16. Ji, X.; Evers, S.; Black, R.; Nazar, L. F. *Nat. Commun.* **2011**, *2*, 325.
17. Jayaprakash, N.; Shen, J.; Moganty, S. S.; Corona, A.; Archer, L. A. *Angew. Chem. Int. Ed. Engl.* **2011**, *50*, 5904.
18. Cai, W.; Li, J.; Zhang, Y.; Xu, G.; Cheng, H. *ChemElectroChem* **2014**, *1*, 1662.
19. Rauchfuss, T. *Nat. Chem.* **2011**, *3*, 648.
20. Chung, W. J.; Simmonds, A. G.; Griebel, J. J.; Kim, E. T.; Suh, H. S.; Shim, I. B.; Glass, R. S.; Loy, D. A.; Theato, P.; Sung, Y. E.; Char, K.; Pyun, J. *Angew. Chem. Int. Ed.* **2011**, *50*, 11409.
21. Wang, J.; Yang, J.; Nuli, Y.; Holze, R. *Electrochem. Commun.* **2007**, *9*, 31.
22. Chung, W. J.; Griebel, J. J.; Kim, E. T.; Yoon, H.; Simmonds, A. G.; Ji, H. J.; Dirlam, P. T.; Glass, R. S.; Wie, J. J.; Nguyen, N. A.; Guralnick, B. W.; Park, J.; Somogyi, A.; Theato, P.; Mackay, M. E.; Sung, Y. E.; Char, K.; Pyun, J. *Nat. Chem.* **2013**, *5*, 518.
23. Pyun, D. C.; Griebel, J. J.; Chung, W. J.; Glass, R.; Norwood, R. A.; Himmelhuber, R.; Simmonds, A. G. U.S. Pat. US20140199592, A1, **2014**.
24. Griebel, J. J.; Nguyen, N. A.; Astashkin, A. V.; Glass, R. S.; Mackay, M. E.; Char, K.; Pyun, J. *ACS Macro Lett.* **2014**, *3*, 1258.
25. Simmonds, A. G.; Griebel, J. J.; Park, J.; Kim, K. R.; Chung, W. J.; Oleshko, V. P.; Kim, J.; Kim, E. T.; Glass, R. S.; Soles, C. L.; Sung, Y. E.; Char, K.; Pyun, J. *ACS Macro Lett.* **2014**, *3*, 229.
26. Griebel, J. J.; Li, G.; Glass, R. S.; Char, K.; Pyun, J. *J. Polym. Sci. A: Polym. Chem.* **2015**, *53*, 173.
27. Griebel, J. J.; Namnabat, S.; Kim, E. T.; Himmelhuber, R.; Moronta, D. H.; Chung, W. J.; Simmonds, A. G.; Kim, K. -J.; van der Laan, J.; Nguyen, N. A.; Dereniak, E. L.; Mackay, M. E.; Char, K.; Glass, R. S.; Norwood, R. A.; Pyun, J. *Adv. Mater.* **2014**, *26*, 3014.
28. Liu, J-g.; Ueda, M. *J. Mater. Chem.* **2009**, *19*, 8907.
29. Liu, J-g.; Nakamura, Y.; Suzuki, Y.; Shibasaki, Y.; Ando, S.; Ueda, M. *Macromolecules* **2007**, *40*, 7902.
30. Okutsu, R.; Ando, S.; Ueda, M. *Chem. Mater.* **2008**, *20*, 4017.
31. Dirlam, P. T.; Simmonds, A. G.; Shallcross, R. C.; Arrington, K. J.; Chung, W. J.; Griebel, J. J.; Hill, L. J.; Glass, R. S.; Char, K.; Pyun, J. *ACS Macro Lett.* **2015**, *4*, 111.
32. Oschmann, B.; Park, J.; Kim, C.; Char, K.; Sung, Y. -E.; Zentel, R. *Chem. Mater.* **2015**, *27*, 7011.

33. Dirlam, P. T.; Simmonds, A. G.; Kleine, T. S.; Nguyen, N. A.; Anderson, L. E.; Klever, A. O.; Florian, A.; Costanzo, P. J.; Theato, P.; Mackay, M. E.; Glass, R. S.; Char, K.; Pyun, J. *RSC Adv.* **2015**, *5*, 24718.

34. Wei, Y.; Li, X.; Xu, Z.; Sun, H.; Zheng, Y.; Peng, L.; Liu, Z.; Gao, C.; Gao, M. *Polym. Chem.* **2015**, *6*, 973.

35. Moad, G.; Rizzardo, E.; Thang, S. H. *Aust. J. Chem.* **2012**, *65*, 985.

36. Moad, G. *Polym. Int.* **2015**, *64*, 15.

37. Moad, G.; Solomon, D. H. The Chemistry of Radical Polymerization, Second Fully Revised Edition, Elsevier Ltd, The Boulevard, Langford Lane Kidlington, Oxford, UK, ISBN 0080442862, 2006, Cap. 9.

38. Salman, M. K.; Karabay, B.; Karabay, L. C.; Cihaner, A. *J. Appl. Polym. Sci.* **2016**, *133*, DOI: 10.1002/app.43655.

39. Hasell, T.; Parker, D. J.; Jones, H. A.; McAllister, T.; Howdle, S. M. *Chem. Commun.* **2016**, *52*, 5383.

40. Crockett, M. P.; Evans, A. M.; Worthington, M. J. H.; Albuquerque, I. S.; Slattery, A. D.; Gibson, C. T.; Campbell, J. A.; Lewis, D. A.; Bernardes, G. J. L.; Chalker, J. M. *Angew. Chem. Int. Ed.* **2016**, *55*, 1714.

41. Evans, A.; Montenegro, M. I.; Pletcher, D. *Electrochem. Commun.* **2001**, *3*, 514.

42. Manan, N. S. A.; Aldous, L.; Alias, Y.; Murray, P.; Yellowlees, L. J.; Lagunas, M. C.; Hardacre, C. *J. Phys. Chem. B* **2011**, *115*, 13873.